

# Solar-blind avalanche photodiodes

Ryan McClintock, Kathryn Minder, Alireza Yasan, Can Bayram, Frank Fuchs<sup>1</sup>, Patrick Kung, and Manijeh Razeghi\*

Center for Quantum Devices; Department of Electrical Engineering and Computer Science;  
Northwestern University; Evanston, Illinois 60208; USA

## ABSTRACT

There is a need for semiconductor based UV photodetectors to support avalanche gain in order to realize better performance and more effectively compete with existing photomultiplier tubes. However, there are numerous technical issues associated with the realization of high-quality solar-blind avalanche photodiodes (APDs). In this paper, APDs operating at 280 nm, within the solar-blind region of the ultraviolet spectrum, are investigated. The devices consist of an  $\text{Al}_{0.38}\text{Ga}_{0.62}\text{N}$  active region grown atop a high quality AlN template layer designed to allow back illumination of the devices through the sapphire substrate. These devices perform well in the unbiased mode of operation. Under the application of large reverse bias these devices show a soft breakdown starting at relatively low electric fields. The devices achieve a maximum optical gain of  $\sim 1000$  at a reverse bias of  $\sim 90$  Volts, which corresponds to an electric field strength of 2.5 MV/cm. The origins of this gain are discussed in detail and modeling of the devices is used to investigate the electric field build up in the multiplication region.

Keywords: APD, AlGaN, Solar-Blind, Detector, Avalanche

## 1. INTRODUCTION

Ultraviolet (UV) photodetectors find uses in numerous applications in the defense, commercial, and scientific arenas. These include, for example, covert space-to-space communications, early missile threat detection, chemical and biological threat detection and spectroscopy, flame detection and monitoring, UV environmental monitoring, and UV astronomy.<sup>1,2,3</sup> Detectors operating in the solar blind region are of special interest. The solar blind region corresponds to the strong atmospheric absorption of solar UV at wavelengths less than 290 nm. This creates a natural low background window for detection of man-made UV sources.

In the past few years, technological and scientific advances in wide bandgap AlGaN based semiconductor materials have led to a renewed interest in AlGaN based UV detectors. The AlGaN material system has a wide direct bandgap and is ideally suited to detection of UV light in the solar blind range, however this material system suffers from several key problems: large dislocation densities, low n-type and p-type doping efficiency (i.e. low conductivity), and lattice and thermal expansion mismatches leading to cracking of the material. All of these problems are exacerbated by the large aluminum compositions necessary to achieve solar-blind photodetectors.

In spite of these challenges, AlGaN has been used to realize efficient solar-blind photodetectors.<sup>4</sup> However, these detectors cannot effectively compete with the existing photomultiplier tube (PMT) based UV detectors. PMTs obtain their high sensitivity by taking advantage of internal gain (typically  $\sim 10^6$ ), however these detectors are bulky, fragile glass tubes that require large biases (typically 1000 V) to operate effectively.<sup>5</sup> It is highly desirable to have a smaller semiconductor-based photodetector capable of realizing this level of sensitivity.<sup>6</sup>

In semiconductors it is possible to obtain internal gain by taking advantage of avalanche multiplication under high electric fields. Unlike photoconductive gain earlier reported in AlGaN based devices,<sup>7</sup> avalanche gain is in principle capable of lower noise and faster response times thus increasing the sensitivity of these photodetectors.

---

<sup>1</sup> On leave from Fraunhofer Institute, Freiburg, Germany, frank.fuchs@iaf.fraunhofer.de

\* razeghi@ece.northwestern.edu; phone 1 (847)491-7251; fax 1 (847)476-1817; <http://cqd.ece.northwestern.edu>

To date, there have been few reports discussing AlGa<sub>N</sub> based APDs. Most of the reports have focused on binary GaN detectors with a cutoff at 364 nm.<sup>8,9,10,11</sup> Most of the discussion of true solar blind AlGa<sub>N</sub>-based APDs has been purely theoretical.<sup>12,13,14</sup> In this paper we report the demonstration of 1000x avalanche gain in AlGa<sub>N</sub>-based solar-blind photodetectors.

## 2. MATERIAL GROWTH AND DEVICE PROCESSING

### 2.1. Material Growth

The material growth and device structure are similar to that discussed in our previous solar blind detector reports.<sup>4,15,16</sup> The devices were grown in an AIXTRON 200/4-HT horizontal flow low-pressure metalorganic chemical vapor deposition reactor. Basal plane (00.1) sapphire was used as the substrate; it was double-side-polished prior to growth in order to allow for the realization of back-illuminated photodetectors. Growth on the sapphire substrate was nucleated with a thin 200 Å low-temperature AlN buffer layer. On top of this a 1 μm template consisting of high quality AlN was grown by atomic layer epitaxy<sup>17</sup> at a temperature of ~1300°C.

On top of this template, an n-type lateral conduction layer consisting of Al<sub>0.5</sub>Ga<sub>0.5</sub>N:Si-In was grown. The silicon-indium co-doping of this layer yields a carrier concentration of  $n \sim 2 \times 10^{18} \text{ cm}^{-3}$  and mobility of  $\mu \sim 60 \text{ cm}^2/\text{V}\cdot\text{s}$ . This layer is several times more conductive than conventional singly-doped AlGa<sub>N</sub>:Si of the same aluminum composition.<sup>15</sup> The use of indium also helps partially relax some of the inherent strain, and allows for the growth of a thicker crack-free conduction layer.

The p-i-n active region consists of 100 nm singly-doped n-type Al<sub>0.45</sub>Ga<sub>0.55</sub>N:Si followed by a 200 nm undoped Al<sub>0.36</sub>Ga<sub>0.64</sub>N absorber region and a 50 nm p-type Al<sub>0.36</sub>Ga<sub>0.64</sub>N:Mg. This is then followed by highly doped p-type GaN:Mg in order to take advantage of the p-GaN/p-AlGa<sub>N</sub> heterostructure and help in the formation of ohmic p-type contacts.<sup>18</sup> A schematic diagram of the complete device structure is shown in Figure 1 below; approximate carrier concentrations are given in the accompanying table. Inspection of the material after growth reveals a smooth crack-free surface.

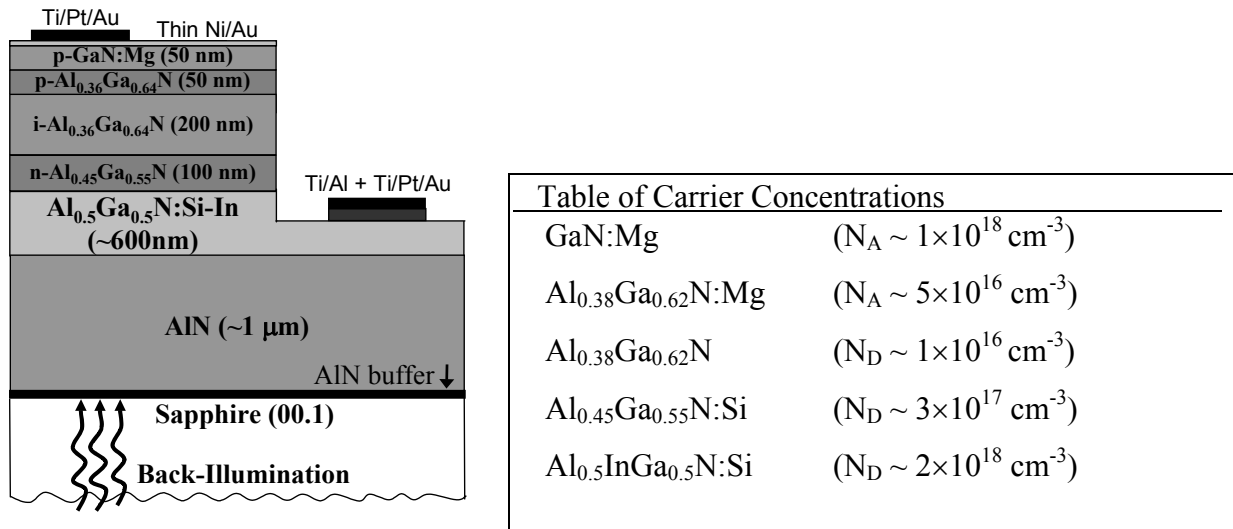


Figure 1. Left.) Schematic cross-section showing the device structure of the back-illuminated APD. Right.) Table of approximate carrier concentrations of the various layers used later in the modeling of this device structure.

## 2.2. Device Processing

The samples are first annealed at 1000 °C for 30 seconds, under dry N<sub>2</sub>, to activate the magnesium in the p-type layers. Then thin layers of 30 Å Ni followed by 30 Å Au are deposited, and annealed under ambient air at 500 °C for 10 minutes, in order to form ohmic contacts to the p-type material on top of the device. The material is then patterned into 25 μm × 25μm square photodetectors using an electron cyclotron resonance (ECR) dry etching system. A common n-type contact consisting of 300 Å Ti / 1800 Å Al is then deposited and annealed under nitrogen to form an ohmic n-type contact to the Al<sub>0.5</sub>Ga<sub>0.5</sub>N:Si-In conduction layer. This contact and the mesas are then covered with a final 400 Å Ti / 300 Å Pt / 1200 Å Au layer in order to facilitate bonding after the annealing. The devices are then covered with 100 nm of SiO<sub>2</sub> to help protect the mesas and prevent premature breakdown of the devices, and windows were opened via wet etching. Indium bumps were deposited on the devices to allow formation of back-illuminated APD arrays, however at this time the devices were only tested individually. A single diode out of the array is shown below in Figure 2.

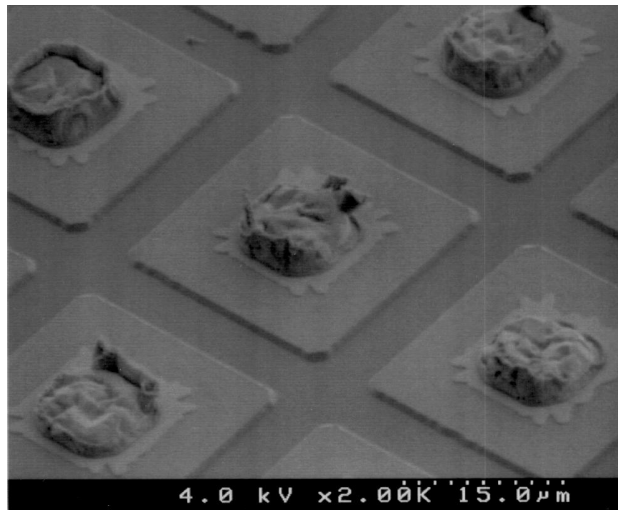


Figure 2. Scanning electron micrograph of an APD after processing. The common n-contact, not shown, is far removed from the mesas to avoid air breakdown of the devices.

## 3. UNBIASED DEVICE PERFORMANCE

### 3.1. Current-voltage characteristics at low bias

First, the current-voltage (I-V) characteristics of these devices are investigated in the dark under small applied bias. These small 625 μm<sup>2</sup> devices have very low dark currents: up to about 10 volts the measurement is limited by the ~10 fA noise floor of the curve tracer used to record these I-V curves. In terms of current density this corresponds to the 1.6×10<sup>-8</sup> A·cm<sup>-2</sup> noise floor observed below in Figure 3.

This dark current density is in sharp contrast to that of larger 1 mm<sup>2</sup> devices fabricated from the same material which typically showed much larger dark current densities, up to 1×10<sup>-3</sup> A·cm<sup>-2</sup>.<sup>4</sup> This scaling of the leakage current more strongly than just with the perimeter or area of the devices indicates that defects play a significant role in the leakage current. This correlates with observations in GaN APDs that the devices require diameters smaller than about 50 μm in order to avoid defect related gain;<sup>9</sup> it is expected that AlGaIn based solar-blind APDs may require devices even smaller to avoid defect related gain. This makes prospects for realizing large area solar-blind APDs difficult without eliminating the catastrophic defects that are almost guaranteed to occur in larger devices. One potential option is to create a large fused array of small detectors, and simply allow the occasional small detector with a catastrophic defect to burn out leaving behind a large effective area device.

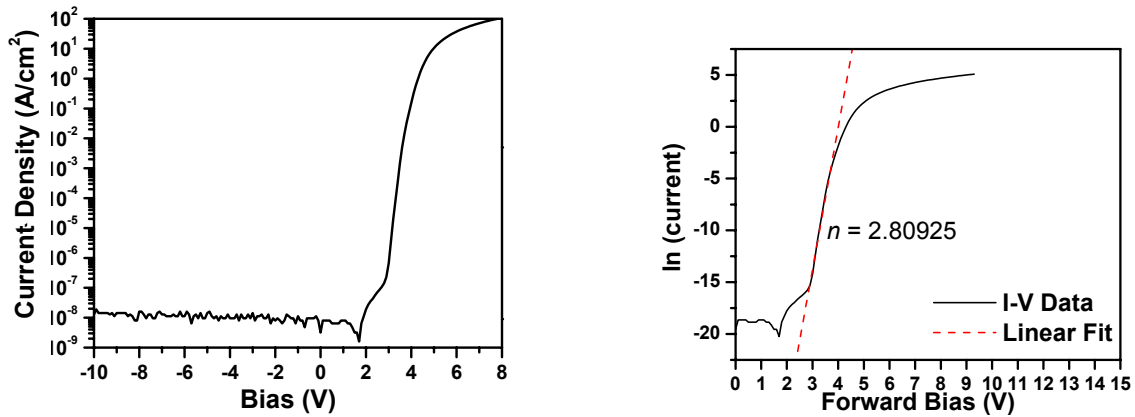


Figure 3. Left) Current-Voltage curve showing the current density in log scale. Right) Natural log of current and fit to linear region used to extract an ideality factor ( $n$ ) of 2.8.

The ideal diode equation, shown below, is used to fit the forward bias data.

$$I_f = C \times \exp\left(\frac{qV}{nkT}\right) \quad \text{Equation 1}$$

This fitting allows the extraction of an ideality factor ( $n$ ), which can provide insight on the conduction mechanisms operating in these photodetectors. The ideality diode equation arises from the combination of the equations for diffusion current and recombination current: the two currents that usually dominate the diode current. The ideality factor is expected to have a value between 1 and 2. Whereas if  $n$  is closer to 1, then diffusion current dominates and if  $n$  is closer to 2 then recombination current dominates. The linear fit shown above in Figure 3 yields an ideality factor of  $n = 2.8$  for this diode. This falls slightly outside of this expected range, but is closer to 2 than most previous devices owing to the high quality of this p-n junction, and minimal contribution from other conduction processes.

### 3.2. Photoresponse

The unbiased photoresponse of these devices was measured using a high intensity xenon arc lamp attached to a monochromator. To allow determination of the absolute responsivity, the system was first calibrated with a Newport-1779 UV-enhanced silicon photodetector masked with a precision calibrated aperture. After calibration of the system, the device was illuminated from the back, through the substrate, and the photoresponse was recorded with a transimpedance amplifier, the output of which was fed to a lock-in amplifier for synchronous detection. The resulting photoresponse is shown in Figure 4.

This device shows an unbiased peak responsivity of 102 mA/W at 280 nm with a FWHM of ~10 nm, which corresponds to a value of 45% for the external quantum efficiency. The absolute response drops three orders of magnitude from the peak into the near-UV region. No contribution from the p-GaN can be seen in the spectral response curve. This confirms that the photoresponse is from the AlGaIn p-i-n structure and not a Schottky junction between the p-GaN and the metal contact.

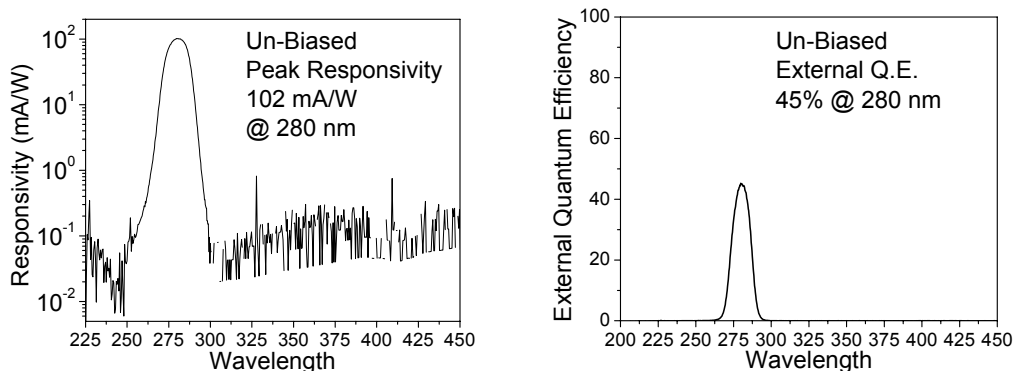


Figure 4. Left) Unbiased responsivity shown in log scale. Right) External quantum efficiency shown in linear scale.

## 4. AVALANCHE MODE DEVICE OPERATION

### 4.1. Current-voltage curves under bias

The I-V curves of these devices were then recorded under reverse biases up of 100 volts. After about 10 volts the dark current comes out of the noise floor and begins to undergo gain and rapidly increase. The same measurement under illumination with broadband white light from the xenon lamp shows a large photocurrent that increases moderately with bias up to about 15 volts and then begins to undergo gain, and rapidly increases with further increasing reverse bias. Both the dark and illuminated I-V curves are plotted in log scale below in Figure 5. These measurements are generally non-destructive, and the same device is consistent from measurement to measurement. The figure below includes error bars from 8 alternating measurements in the illuminated and dark conditions. It can be seen that at voltages approaching 100 volts the dark current and illuminated current begin to converge; this occurs as additional dark current gain compounded with leakage of the devices eclipses the photocurrent gain.

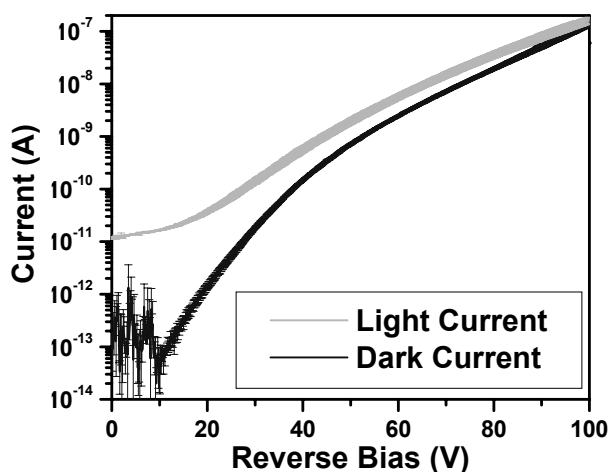


Figure 5. Current-voltage behavior as a function of applied reverse bias, both under illumination and in the dark. Errors bars have been added to indicate the variation over 4 consecutive pairs of alternating light-dark measurements of the same diode.

The avalanche gain (M) is defined as the difference between the primary multiplied current and the multiplied dark current, normalized by the difference between the primary unmultiplied current and the unmultiplied dark current. The gain can be calculated from Figure 5 above using Equation 2 below.

$$M = \frac{I_{\text{Illuminated}}(V) - I_{\text{dark}}(V)}{I_{\text{Illuminated}}(0) - I_{\text{dark}}(0)} \quad \text{Equation 2}$$

The unmultiplied currents are taken from the flatter portion of the curves prior to the onset of avalanche gain. The calculated photocurrent and the corresponding gain (M) are shown below in Figure 6.

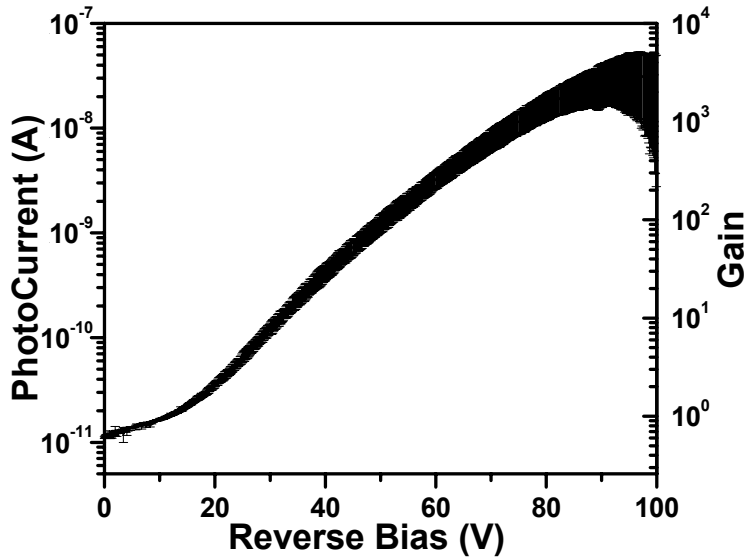


Figure 6. Calculated photocurrent (left axis) and corresponding gain (right axis) from the data of Figure 5. Error bars indicate +/- 1 standard deviation.

These devices show a soft avalanche breakdown starting at ~15 volts. The gain then increases exponentially until saturating at a gain of greater than ~1000 at a reverse bias of ~90 volts. These devices never develop a sharp Geiger mode breakdown. This is in contrast to the results typical of GaN APDs where the gain tends to hold off until larger voltages and then rapidly increases exhibiting a hard Geiger mode breakdown.

In GaN APDs the ionization coefficients for holes and electrons are believed to be very similar at the breakdown field strength.<sup>19</sup> This means that both carriers contribute to the gain and help to support the hyper-exponential Geiger mode breakdown of these devices shortly after the onset of gain. However, this is not necessarily the case for all materials, and if the ionization coefficients differ significantly, only a single carrier may support gain at the electric fields present within the device. If this is the case then the gain is expected to increase geometrically and would never show a Geiger mode breakdown. This may be the cause of the soft avalanche breakdown and absence of a hard ‘breakdown voltage’ in our devices. And, it may mean that significant improvement to the device performance can be realized by implementing a separate amplification and multiplication (SAM) structure that would ensure that only the gain dominating carrier is injected in the multiplication region.

#### 4.2. Device Modeling

Using a 1D finite element model<sup>20</sup>, we investigated the electric field build-up in the multiplication region. The doping concentrations used in the model were given with the structure in Figure 1. These doping concentrations are estimates

inferred from Hall measurements of independent layers used for calibration of the structure, however the actual active carrier concentrations in the device as grown may differ slightly. This model also neglects the piezoelectric fields due the strained layers. Plots of the evolution of the modeled electric field profile are shown in Figure 7 below.

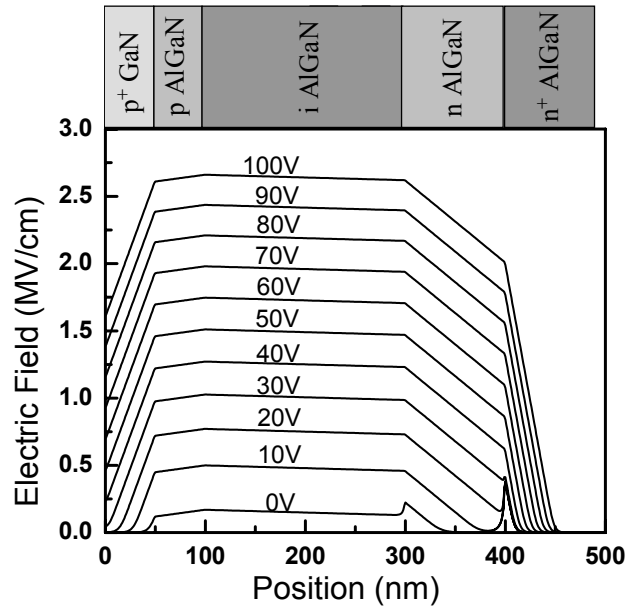


Figure 7. Electric Field Profile under various applied reverse biases.

From this model it is possible to estimate the electric field at the onset of gain to be only  $\sim 5 \times 10^5 \text{ V}\cdot\text{cm}^{-1}$  which increases to  $\sim 2.5 \times 10^6 \text{ V}\cdot\text{cm}^{-1}$  when the gain begins to saturate. However, it is expected that the peak electric field may be significantly larger due to inhomogeneity of the doping, and ionized defects. This model only considers the average electric field in the plane of the device.

This model reveals that the electric field is not well confined to the gain region. This is due to the difficulty of achieving highly doped AlGaN. This means that the peak electric field remains rather small in spite of the large applied reverse bias. It also means that electric field is high enough to support gain outside of the intended multiplication region. The effective multiplication region is closer to 300 nm wide rather than the designed 200 nm.

Physically, avalanche gain is a function of the ionization coefficient ( $\alpha$ ) and multiplication width ( $W$ ). This behavior can be fitted using an empirical equation that models the ionization coefficient with two fitting parameters  $\alpha_0$  and  $C$ .<sup>21</sup>

$$M = \exp(W \cdot \alpha) = \exp\left\{W \cdot \alpha_0 \cdot \exp\left\{\frac{-C \cdot W}{V}\right\}\right\} \quad \text{Equation 3}$$

The multiplication region width is chosen as 300 nm rather than the designed 200 nm in response to the electric field profile model above. This model provides a good fit to the avalanche gain data with the fitting parameters  $C = 2 \text{ MV/cm}$ ,  $\alpha_0 = 4.9$ . Figure 8 below shows good agreement of the theory (dashed) and experimental (solid) data up to 90 volts where gain saturation takes over.

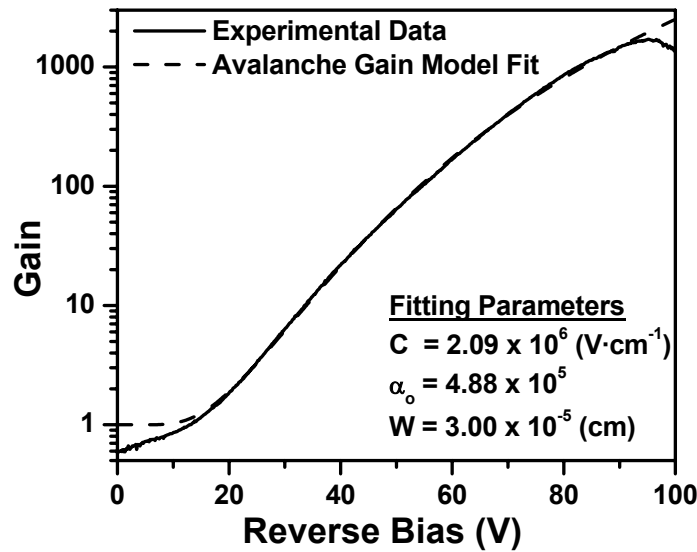


Figure 8. Avalanche gain model of the device. The solid curve shows the experimental data, the dashed curve shows the model.

#### 4.3. Ruling out other origins for the gain

The diodes fit well with an avalanche gain model, however it is worthwhile to rule out other possible origins of the gain observed in these devices. There are three main gain mechanisms that could be responsible for the large gain observed in these devices: avalanche multiplication, Zener tunneling, and photoconductive gain.

In order to rule out Zener tunneling the temperature dependence of the dark current gain in these devices is investigated (shown below in Figure 9). The temperature-dependent dark current shows a large positive temperature coefficient, and a thermal activation energy of  $\sim 240$  meV can be extracted from this evolution. This strong temperature dependence observed below rules out the temperature-insensitive process of Zener tunneling as the dominant gain mechanism.

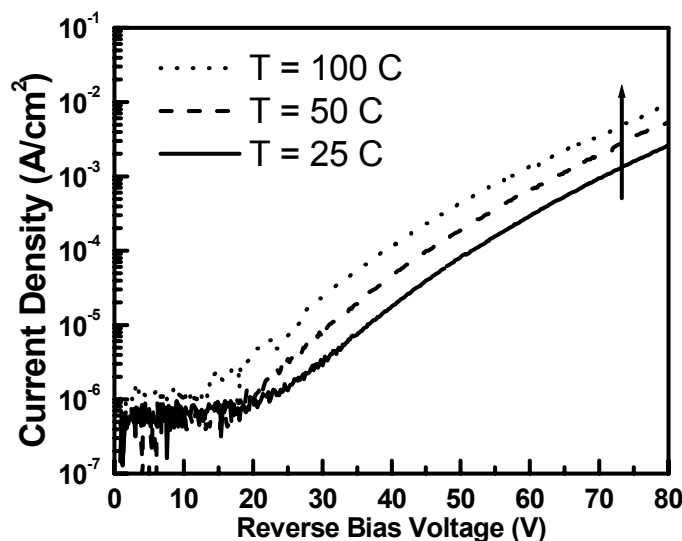


Figure 9. Dark current reverse bias current-voltage data at several different temperatures, showing the temperature dependence of the dark current gain.

Photoconductive gain can also be ruled out based on the shape and magnitude of the gain observed. If photoconductive gain were the dominant gain mechanism, then the gain would be expected to increase linearly with voltage.<sup>22</sup> Instead, in Figure 6, it can be seen to increase exponentially. This allows us to rule out Zener tunneling and photoconductive gain, and together with the avalanche gain model fit allows us to attribute the gain to avalanche multiplication of carriers inside the device.

## 5. CONCLUSION

We have demonstrated AlGaIn based solar-blind avalanche photodiodes with a gain in excess of 1000 at 90 volts of reverse bias. This gain can be attributed to avalanche multiplication of the photogenerated carriers within the device, and shows good agreement with that model. Modeling of the electric field build up indicates that the maximum gain occurs at a peak electric field strength of 2.5 MV/cm. However at higher fields, the gain has to compete with the large simultaneous dark current gain. This leads to the photocurrent gain saturating and then decreasing at voltages larger than ~90 volts. This gain saturation prevents the device from exhibiting a strong Geiger mode breakdown, and may limit the ability of these devices to operate in a photon counting mode. These devices show the potential of AlGaIn based APDs, and with further improvement of the material, and sufficient device optimization, it may be possible to achieve devices with sensitivities approaching those of commercial PMTs.

## ACKNOWLEDGMENTS

The authors of this paper would like to acknowledge Dr. Bijan Movaghar for many helpful discussions regarding this work. We would also like to acknowledge Dr. Henryk Temkin for his support and encouragement.

## REFERENCES

1. P. Kung, A Yasan, R. McClintock, S.R. Darvish, K. Mi, M. Razeghi, "Future of Al<sub>x</sub>Ga<sub>1-x</sub>N materials and device technology for ultraviolet photodetectors", Proc. SPIE, vol. **4650**, pp.199-206, (2002).
2. M. Razeghi, "Short-wavelength solar-blind detectors- status, prospects, and markets", Proc. IEEE, vol. **90**, pp. 1006-1014, (2002).

- 
3. M. Ulmer, M. Razeghi, E. Bigan, "Ultra-Violet Detectors for Astrophysics, Present and Future," Proc. SPIE vol. **2397** pp. 210-216, (1995).
  4. R. McClintock, A. Yasan, K. Mayes, D. Shiell, S. R. Darvish, P. Kung, and M. Razeghi, "High quantum efficiency AlGa<sub>N</sub> solar-blind p-i-n photodiodes", Appl. Phys. Lett. **84**, 1248 (2004).
  5. Hamamatsu Photonics, K.K., <http://usa.hamamatsu.com/>, PMTs based upon Cs-Te photocathodes such as R1080.
  6. DARPA BAA06-14, Deep Ultraviolet Avalanche Photodetectors (DUVAP), (2005)
  7. J. L. Pau, E. Monroy, M. A. Sánchez-García, E. Calleja, and E. Munoz, "AlGa<sub>N</sub> ultraviolet photodetectors grown by molecular beam epitaxy on Si(111) substrates", Materials Science and Engineering B **93**, 159 (2002).
  8. K. McIntosh, R. Molnar, L. Mahoney, M. Geis, K. Molvar, I. Melngailis, R. Aggarwal, W. Goodhue, S. Choi, and D. Spears, "Ga<sub>N</sub> avalanche photodiodes grown by hydride vapor-phase epitaxy" Appl. Phys. Lett. **75**, 3485 (1999).
  9. J. Carrano, D. Lambert, C. Eiting, C. Collins, T. Li, S. Wang, A. Beck, R. Dupuis, and J. Campbell, "Ga<sub>N</sub> avalanche photodiodes" Appl. Phys. Lett. **76**, 924 (2000).
  10. B. Yang, T. Li, K. Heng, C. Collins, S. Wang, J. Carrano, R. Dupuis, J. Campbell, M. Schurman, and I. Ferguson, "Low dark current Ga<sub>N</sub> avalanche photodiodes", IEEE J. Quantum Electron. **36**, 1389 (2000).
  11. S. Verghese, K. McIntosh, R. Molnar, L. Mahoney, R. Aggarwal, M. Geis, K. Molvar, E. Duerr, and I. Melngailis, "Ga<sub>N</sub> avalanche photodiodes operating in linear-gain mode and Geiger mode", IEEE Trans. Elect. Dev. **48**, 502 (2001).
  12. Y. Wang, K. Brennan, and P. Ruden, "Theoretical study of a potential ultraviolet avalanching detector based on impact ionization out of confined quantum states", IEEE J. Quantum Electron. **27**, 232 (1991).
  13. P. Ruden and S. Krishnankutty, "A solar blind, hybrid III-nitride/silicon, ultraviolet avalanche photodiode", IEEE Trans. Elect. Dev., **46**, 2348 (1999).
  14. C. Sevik and C. Bulutay, "Gain and temporal response of AlGa<sub>N</sub> solar-blind avalanche photodiodes: An ensemble Monte Carlo analysis" Appl. Phys. Lett. **83**, 1382 (2003).
  15. R. McClintock, A. Yasan, K. Mayes, D. Shiell, S.R. Darvish, P. Kung, and M. Razeghi, "High Quantum Efficiency Solar-Blind Photodetectors", Proc. SPIE **5359**, 434 (2004).
  16. R. McClintock, K. Mayes, A. Yasan, D. Shiell, P. Kung, and M. Razeghi, "320×256 solar-blind focal plane arrays based on Al<sub>x</sub>Ga<sub>1-x</sub>N" Appl. Phys. Lett. **86**, 011117-1 (2005).
  17. J. Zhang, H. Wang, W. Sun, V. Adivarahan, S. Wu, A. Chitnis, C. Chen, M. Shatalov, E. Kuokstis, J. Yang, and M. Asif Khan, "High-quality AlGa<sub>N</sub> layers over pulsed atomic-layer epitaxially grown AlN templates for deep ultraviolet light-emitting diodes", J. Elect. Mat. **32**, 364 (2003).
  18. M. Razeghi, US Patent **5831277**, (1997).
  19. I. Oguzman, E. Bellotti, K. Brennan, J. Kolnik, R. Wang, and P. Ruden, "Theory of hole initiated impact ionization in bulk zincblende and wurtzite Ga<sub>N</sub>", J. Appl. Phys. **81**, 7827 (1997).
  20. D. Winston and R. Hayes, "SimWindows - A New Simulator for Studying Quantum-well Optoelectronic Devices" Compound Semiconductors 1994 Institute of Physics Conference Series **141**, 747 (1995).
  21. G. Stillman and C. Wolfe, "Avalanche Photodiodes" in "Semiconductors and semimetals", edited by R. Willardson (Academic Press, New York, 1977), Vol. **12**, Chap. 5, p.304.
  22. S. Sze, "Physics of Semiconductor Devices", 2nd edition (John Wiley & Sons, New York, 1981), Chap. 13, p.744.